Nonequilibrium Remodeling of Collagen IV Networks *in Silico*

Billie Meadowcroft,[1,2,3,4] Valerio Sorichetti,[1] Eryk Ratajczyk,[4,5,6] Fernanda Pérez-Verdugo,[1] Nargess Khalilgharibi,[2,3] Yanlan Mao,[2,3] Ivan Palaia,[1,7] and Anđela Šarić[1,*]

[1]*Institute of Science and Technology Austria, Klosterneuburg, Austria*

[2]*UCL Laboratory for Molecular Cell Biology, University College London, Gower Street, London WC1E 6BT, United Kingdom*

[3]*Institute for the Physics of Living Systems, University College London, Gower Street, London WC1E 6BT, United Kingdom*

[4]*Department of Physics and Astronomy, University College London, London WC1E 6BT, United Kingdom*

[5]*Rudolf Peierls Centre for Theoretical Physics, University of Oxford, Parks Road, Oxford OX1 3PU, United Kingdom*

[6]*Kavli Institute for Nanoscience Discovery, University of Oxford, South Parks Road, Oxford OX1 3QU, United Kingdom*

[7]*Department of Physics, King's College London, London WC2R 2LS, United Kingdom*

(Received 11 October 2024; accepted 28 April 2025; published 5 September 2025)

Collagen IV is one of the main components of the basement membrane, a layer of material that lines the majority of tissues in multicellular organisms. Collagen IV molecules assemble into networks, providing stiffness and elasticity to tissues and informing cell and organ shape, especially during development. In this work, we develop two coarse-grained models for collagen IV molecules that retain biochemical bond specificity and coarse grain at different length scales. Through molecular-dynamics simulations, we test the assembly and mechanics of the resulting networks and measure their response to strain in terms of stress, microscopic alignment, and bond dynamics. Within the basement membrane, collagen IV networks rearrange by molecule turnover, which affects tissue organization and can be linked with enzyme activity. Here we explore network rearrangements via bond remodeling, the process of breaking and remaking of bonds between network molecules. We then investigate the effects of active (enzymatic) bond remodeling. We find that this nonequilibrium remodeling allows a network to keep its integrity under strain, while relaxing fully over a variety of timescales, a dynamic response that is unavailable to networks undergoing equilibrium remodeling.

DOI: 10.1103/gdd5-rnh7

I. INTRODUCTION

Mechanical properties of tissues originate from the constituent cells and their interactions, as well as the surrounding medium: the extracellular matrix (ECM). The basement membrane (BM) is a specialized type of ECM that lines epithelial tissues in all multicellular organisms [1,2].

The BM's mechanics, mostly due to networks of collagen IV, likely plays a crucial role in shaping cells and tissues during development, homeostasis, and aging [3,4]. For example, it has recently been shown that the tissue shape in the developing *Drosophila* egg is instructed by BM stiffness: Softer BM at the poles of the egg triggers local changes in cell orientations [5]. The BM mechanics has also been related to aging in humans whereby older BMs are stiffer [6] and are associated with an accumulation of collagen IV [7].

It is thought that the ECM and in particular the BM behave viscoelastically under applied stress [8–11]. A viscoelastic material deforms elastically on short timescales, without retaining memory of the deformation history. On long timescales, however, it can flow like a liquid [12]. In polymeric materials, viscoelastic behavior can be caused by entanglements [13–17] or by the breaking and reforming of physical or chemical bonds, which leads to network remodeling. We hereafter use the term *remodeling* to refer to network rearrangement due to the breaking and reforming of bonds. Polymer networks that remodel in this way have been studied by soft-matter physicists for decades, due to their mechanical strength, their processability, and their ability to self-heal [18–22]. Examples are materials based on hydrogen bonds [23], metal ligands [24], and dynamic covalent bonds [25–28]. Dynamic bond remodeling is also found in many biological components such as microtubule networks [29,30] and actomyosin gels [31,32], where cross-linkers bind and unbind from filaments, and even in multiorganism systems such as fire ant rafts [33].

It is challenging to determine the extent of collagen IV network remodeling in tissues, but collagen IV turnover within the ECM could be an appropriate proxy [34]. Turnover, measured as the half-life of a collagen IV molecule within the ECM, is known to play a role in development [35], aging [36], and disease [37–40]. Vastly different values of collagen IV lifetimes have been reported in the literature, suggesting that the mechanism for degradation and/or replacement of molecules may vary for different systems [34,35,41]. For example, finite lifetimes within a network could be the result of breaking and reforming bonds between collagen IV molecules, with newly formed molecules possibly replacing

*Contact author: andela.saric@ist.ac.at

the old [42]. Turnover has been associated with changes in tissue shape [42] and in most studies it was found to be intimately linked to enzymes such as collagenases [42–44]. Several studies show that collagen IV cleaving enzymes are upregulated or downregulated during development or disease [45–47]. Linking the activity of enzymes and network remodeling dynamics therefore may be crucial for understanding the mechanics and viscoelastic properties of ECM components [11,48] and their subsequent role in the shape and dynamics of tissues [45,49].

The mechanics and dynamics of collagen IV networks are largely understudied, as are the microscopic mechanisms of collagen IV cleaving enzymes. Conversely, the collagen IV molecule structure and bonding topology have been well established since the 1990s. The collagen IV units, which bond to make up a network, are called protomers. A collagen IV protomer is made up of three distinct domains: the NC1 domain at one end, the 7S domain at the other end, and a 390-nm-long triple helix connecting them [50,51] [Fig. 1(a)]. The single protomers bind one another at their ends and assemble into thin sheets [52] [Fig. 1(c)]. In particular, the NC1 ends of two protomers can come together to form an NC1 bond [53,54] and the 7S ends of up to four protomers can form 7S bonds [55–58] [Fig. 1(b)]. Despite genetic similarities with the much more studied collagen I, the structures formed by collagen I and by collagen IV, as well as their binding mechanisms, are considerably different. Collagen I protomers form long fibrils that stick laterally to each other, assembling into thick, fairly rigid fibers [59–62], while collagen IV protomers bind through their ends, not forming fibrils or fibers but rather thin flexible nets. Although lattice models have been proposed to interrogate collagen IV network mechanics [63,64], a model incorporating the known molecular details of collagen IV and its bonding is still missing.

In this work, we seek to understand how the microscopic properties of the collagen IV protomer, and most importantly its binding specificity, determine the structure and the mechanical response of the self-assembled networks. We propose two computational models for collagen IV, with different levels of coarse graining [65]. The first model describes a protomer as a semiflexible polymer, with ends decorated by specific binding sites [Figs. 1(d)–1(f)]. We use it to study the role of the flexible central chain in network formation. The second model coarse grains the whole protomer chain to an entropic spring while retaining bond specificity [Figs. 1(g)–1(i)]. This allows us to reach length scales which are probed in microscopy experiments and to distill how bond kinetics determines macroscopic network properties [3].

To understand the possible role of enzymes in network remodeling, we then compare two different routes for bond rupture and formation, using the coarser bond topology model. One route, termed the equilibrium protocol, locally obeys detailed balance [66], while the other route, termed enzymatic protocol, does not. We find that active (enzymatic) remodeling brings the network to relaxed states which are forbidden under equilibrium remodeling. Our results provide an example of a scenario in which active processes strongly affect the structure and mechanics of self-assembled materials [67–71].

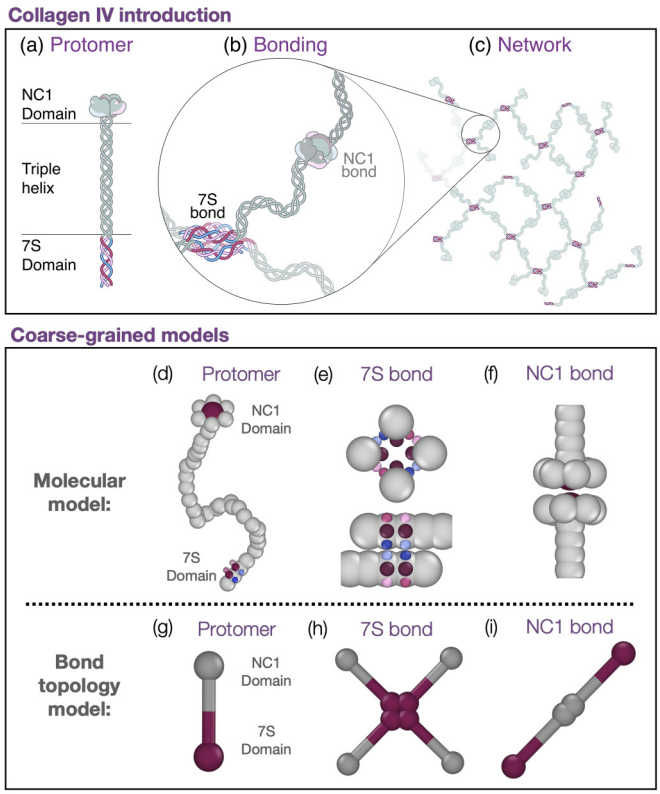

FIG. 1. Collagen IV bonding and models. (a) A collagen IV protomer is made up of a triple helix with an NC1 domain at the C terminus of the helical chains and a 7S domain at their N terminus. (b) The NC1 end bonds with one other collagen IV protomer to form an NC1 bond. The 7S end can bond with up to three other collagen IV protomers to form a 7S tetrameric bond. (c) Sheetlike collagen IV network. (d) The molecular model is a bead-spring model where the protomer is made up of 37 beads (with seven constituting the NC1 domain) connected by springs. The binding regions of the 7S domain are modeled using attractive patches. (e) The 7S end forms bonds via six interacting patches arranged such that four ends can form a stable bond. (f) The NC1 end forms bonds via one interacting patch, surrounded by a ring of six beads with volume exclusion, to prevent more than two NC1 ends from binding. (g) In the bond topology model a collagen IV protomer is represented by two interacting ends connected by a rigid rod with no volume exclusion. (h) The 7S end can bond with three other protomers to form the 7S bond. (i) The NC1 end can bond with one other protomer to form the NC1 bond.

II. MODELS AND SIMULATION METHODS

Here we present the two particle-based models, each simulated using molecular dynamics.

The molecular model represents a protomer (including the triple helix and the binding domains) as a semiflexible chain made of spherical beads connected by harmonic springs [Fig. 1(d)]. Short-range attractive patches ensure the 7S end of the protomer bonds with two antiparallel protomers on their 7S ends, which in turn bond with a fourth parallel protomer on its 7S end, as proposed in the literature [55,72] [Fig. 1(b)]. This results in the formation of dimers, trimers, or at most tetramers, as depicted in Fig. 1(e) [58]. The attractive site at the other end, protected by six inert beads to ensure one-to-one binding, represents the bulkier NC1 domain and bonds

with the NC1 end of another protomer, forming the dimer depicted in Fig. 1(f) [53,54]. Volume exclusion ensures no chain crossing can take place so that entanglement between chains is correctly captured.

The molecular model, as per its name, has the advantage of providing a more direct connection to the molecular details of the system. However, despite its simplicity, simulating a system size that can be directly compared to conventional microscopy data is still not feasible due to prohibitively large computational times.

To simulate networks which are closer to the typical experimental sample sizes and timescales [3], we developed the bond topology model, which represents each molecule using two beads only. This is reminiscent of other recent efforts at reducing the complexity of elastomer network models by mapping full polymer systems to simplified mesoscale models [22]. Few parameters define the length and energy scales of the protomer and its bonding within this model, and each is chosen in such a way to coarse grain a key aspect of the molecular model. The parameter choice is discussed in detail in Sec. I of the Supplemental Material (SM) [73].

In the bond topology model, a protomer is represented as a two-beaded rod, as shown in Fig. 1(g). The 7S bead can bond with beads of the same kind from up to three other protomers [Fig. 1(h)], while the NC1 bead can bond with the NC1 bead of only one other protomer [Fig. 1(i)]. Rods are treated as rigid bodies and the flexibility of the chain is effectively encoded in the harmonic angle potentials that make up the 7S and NC1 bonds. The bonding distance is imposed by a two-body harmonic potential, whereas a three-body harmonic potential controls the angular flexibility of the bonds between two protomers. A collagen network is therefore defined only through its bond topology and through the distance that protomers impose between binding sites.

For both models, parameters are chosen such that the majority of the protomers spontaneously assemble into a percolating network. The network structure is however not fixed: Bonds are dynamic and can break and reform due to thermal fluctuations. We first consider passive remodeling (Secs. III A and III B). In the molecular model, bonds are formed and broken through attractive interactions, according to the equilibrium canonical distribution, sampled using molecular dynamics. The strength of the attraction determines the bond remodeling dynamics. In the bond topology model, the molecular dynamics is coupled with a Metropolis algorithm [74] that explicitly breaks and forms bonds locally respecting detailed balance, thus changing connectivity while locally preserving equilibrium [Fig. 4(a)]. Then, in Sec. III C, we introduce active bond remodeling for the bond topology model. For this purpose we modify the algorithm in breach of detailed balance so that bonds break and form either randomly or with a distance-dependent rule, as further explained in Sec. III C [Fig. 4(b)].

Particle motion is the result of overdamped Langevin dynamics [75], so the solvent is treated implicitly and hydrodynamics is neglected. Simulations are performed in LAMMPS [76] and visualized using OVITO [77]. The simulation length unit is a and the simulation timestep is Δt. The REACTER package [78] is used for the bond topology model. Further details on the models, simulation setup, and parameters are outlined in Sec. I of the SM [73].

III. RESULTS

A. Self-assembly

We first set out to explore how the collagen IV protomers self-assemble into networks in the absence of external strain. The simulations begin with the protomers in a random configuration, from which they freely diffuse and bond/unbond with other protomers until the system reaches a steady state, as shown in the snapshots in Figs. 2(a) and 2(d) and SM Videos 1 and 2 [73].

We analyze the connectivity of these networks by calculating the percentage of protomers in the largest connected cluster f_{LC}, which gives a measure of network connectivity. In both models the binding energy of the protomer-protomer bonds is varied to identify the percolation threshold. We thereafter choose bond energies to be above this threshold such that we only investigate percolating networks (see Fig. S9 in the SM [73]). Figures 2(b) and 2(f) show f_{LC} as a function of time for networks that become fully connected. Note that the simulation time step Δt corresponds to a larger physical time in the case of the more-coarse-grained, lower-density, bond topology model (see Sec. IV of the SM [73]).

Both models form networks that on average form a total of $B = 3$–3.2 bonds per protomer, as shown in Figs. 2(c) and 2(f). This is significantly below the value of $B = 4$ which would indicate that all bonds are satisfied and corresponds to the system's ground state. Experimental studies of collagen IV assembly have indicated a value $B \approx 3.2$ bonds per protomer from *in vitro* low-concentration essays [58] and $B \approx 3$ from eye tissue imaging [79]. However, the connectivity of collagen IV networks within the basement membrane is unknown. In our models, the value of $B \approx 3$–3.2 bonds per protomer is maintained when bond strength is increased (Figs. S9C and S9D in the SM [73]), suggesting that long-lived bonds act as kinetic traps that prevent the system from reaching full connectivity.

In the bond topology model, we additionally monitor how the 7S tetramer bonds form. Figure 2(e) shows typical snapshots of the 7S bonding pathway. In Fig. 2(g) we see 70% of tetramers and trimers make up the percolating network, while 30% of the 7S bonds are still in the dimer configuration. Overall, these result validate the two models, which are in line with each other and corroborate the available experimental data.

B. Mechanics

To investigate the mechanics of the self-assembled networks, we apply a step strain and monitor the response of the networks to this strain. The strain is applied over a short time interval and over one direction, similar to those applied in experiments probing the mechanics of tissues in fly wing discs. For example, manual stretchers have been used to strain the wing disc by up to 100%, while the cells can be imaged as they respond to the perturbation [80]. The strain protocol is represented in Figs. 3(a) and 3(b) (see also Sec. II of the SM [73] for details). The snapshots in Figs. 3(c) and 3(d) show the networks before, immediately after, and some time after the strain is applied. The stretching process is also shown in SM Videos 3 and 4 [73]. The macroscopic mechanical response of

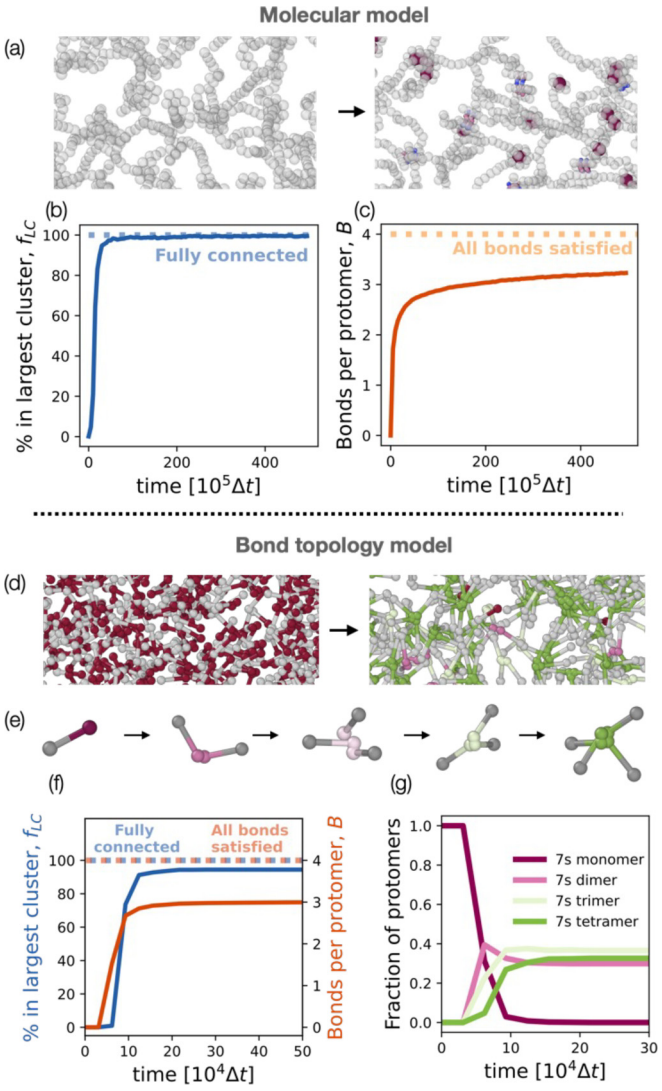

FIG. 2. Network self-assembly. The molecular model and the bond topology model both self-assemble into percolating networks. (a) Snapshots of the molecular model before (left) and after (right) the network self-assembles. The molecule ends are shown with color if they are bonded [colored as in Figs. 1(d)–1(f)]. (b) Percentage of molecules in the largest connected network f_{LC} over time. The network percolates after a time $5 \times 10^6 \Delta t$. (c) Number of bonds per protomer in time, saturating to 3.2. If all bonds were satisfied the number of bonds per protomer would be 4 (1 from the NC1 domain and 3 from the 7S domain). (d) Snapshots of the bond topology model before (left) and after (right) self-assembly. (e) Pathway for the bonding of 7S ends, which are colored according to the degree of bonding as shown in the legend (g). (f) Percentage of molecules in the largest cluster and the bonds per protomer in time. The network percolates after $1.0 \times 10^5 \Delta t$ and the number of bonds per protomer saturates to 3. (g) Time evolution of the formation of 7S bonds by the number of bonding partners. The 7S dimer bonds are the first to form, but over long times the 7S tetramer and trimer bonds dominate.

the network is studied by measuring stress in the direction of strain. The microscopic response is examined by measuring the individual protomer alignment with the direction of strain and by characterizing the bond kinetics.

The stress response σ_{zz}, with z the direction of strain, is shown in Figs. 3(e) and 3(f). In both models, the stress peaks once the final strain is reached and then decreases over time as the strain is kept constant. This underlies the viscoelastic nature of the material, with an elastic response at small timescales (linear increase of stress upon linear increase of strain) followed by a viscous relaxation at large timescales (stress relaxation at constant strain). The stress relaxation of the material is well described by a two-mode generalized Maxwell model [12], i.e., $\sigma_{zz}(t) = \Delta\sigma_{zz}[f \exp(-t/\tau_1) + (1-f)\exp(-t/\tau_2)]$, where $\Delta\sigma_{zz}$ is the increase of stress upon stretch, τ_1 is the fast relaxation mostly due to protomer rearrangement in space, and τ_2 is the slow relaxation due to the bond remodeling. We further characterize the Young modulus and the critical strain, the onset of strain stiffening [81], of the bond topology model networks in Sec. III of the SM [73]. A small-strain analysis results in a Young modulus that is small when converting to standard units (0.03 Pa) compared to measurements of three-dimensional networks of other ECM components [8]. This possibly reflects the thin semi-two-dimensional nature of the networks simulated here and suggests that the noncollagen IV components of the BM might play a key role at small strain or that the *in vivo* collagen IV matrix might be prestressed during development.

To gain insight in how viscoelasticity emerges from the microscopic rearrangement of protomers, we look at single-protomer alignment, which we define by $\cos^2\theta$, where θ is the angle between the protomer end-to-end axis and the direction of strain. We measure the average alignment over all protomers, $\phi = \langle\cos^2\theta\rangle$, in Figs. 3(g) and 3(h). Completely random alignment corresponds to $\phi = 1/3$. We see that the macroscopic stress response is reflected in the microscopic alignment response: The alignment also peaks when the final strain is reached and slowly decays as the strain is kept constant. From the qualitative agreement between the molecular model and the bond topology model, we deduce that entanglement between molecules, which could slow down the dynamics and stress relaxation by orders of magnitude [13,15,17,82], is negligible in the molecular model, at least for these densities. This justifies the choice to neglect excluded-volume effects in the bond topology model.

As both models have nonpermanent bonds, we examined whether there is a change in the bonding dynamics in response to the applied strain. Figures 3(i) and 3(j) show measurements of the bonds broken and made per time step for each model. In both cases, after strain is applied, temporarily more bonds are broken than made. Balance is quickly restored, as new, unstressed, bonds are formed.

Taken together, the networks behave elastically on a short timescale in response to external strain, generating stress. This stress induces sudden but persisting alignment of protomers in the direction of strain and is successively relieved, on longer timescales, by bond breaking and remaking. These results connect the macroscopic viscoelastic response of the networks to the microscopic network arrangement and bond remodeling dynamics. The stress relaxation mechanism measured here is analogous to that observed in other polymer networks with reversible bonds [21,22,28]. In particular, the correlation between stress and molecular alignment relaxation was also reported in simulations of vitrimers [28].

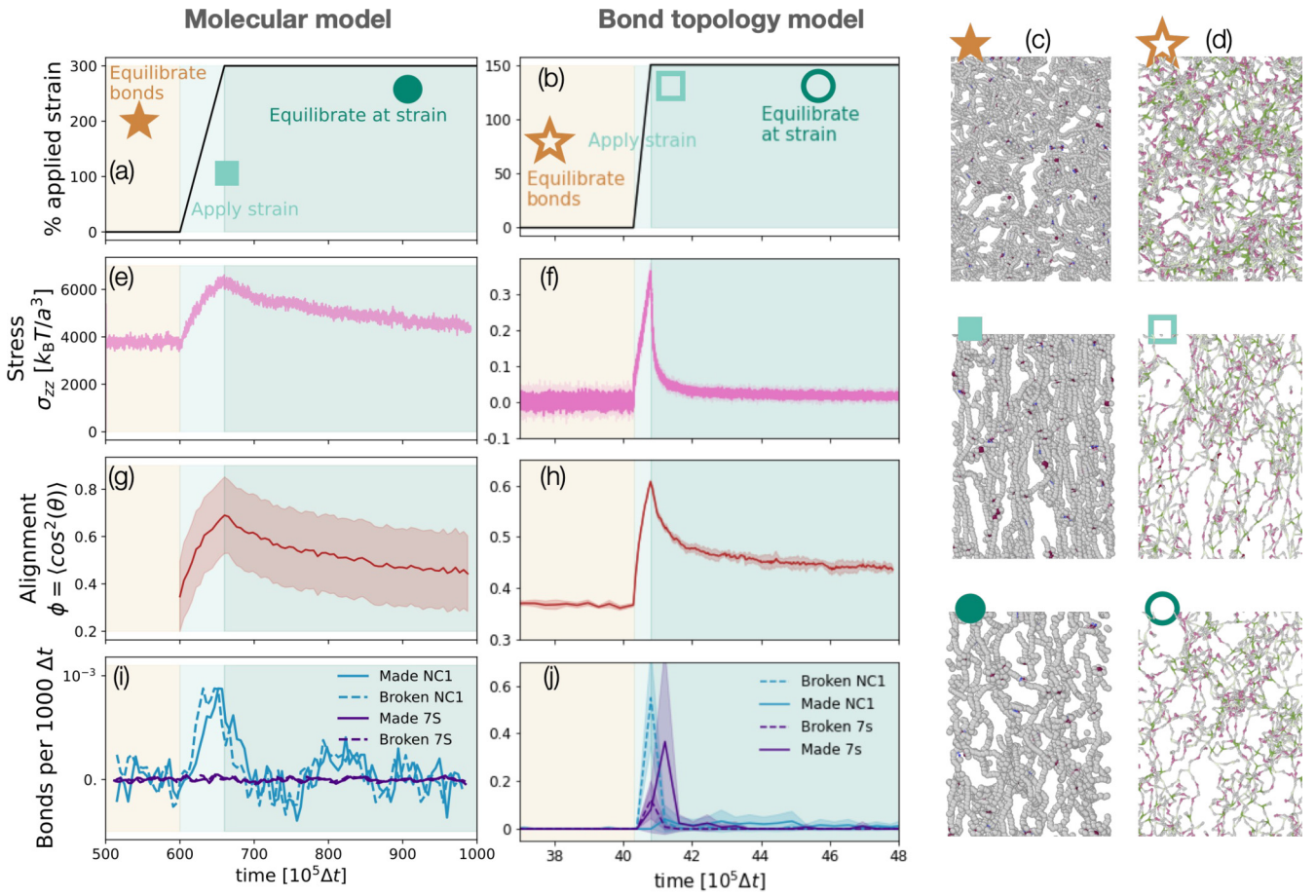

FIG. 3. Mechanical response to strain. (a) and (b) The networks are subject to strain after equilibration. (a) The molecular model is subject to a strain of 300% in the z direction, which is applied at constant volume. (b) The bond topology model is subject to a strain of 150% in the z direction where the box size is kept constant in the x and y directions. Shown are snapshots of (c) the molecular model and (d) the bond topology model before strain is applied (★), immediately after strain is applied (■), and after network relaxation (●). The stress in the direction of strain is plotted over time in (e) the molecular model and (f) the bond topology model. The stress reaches a peak at the end of the strain application and then relaxes while the strain is kept constant. (g) and (h) Protomer alignment with respect to the direction of strain, averaged over all protomers. (i) and (j) Number of bonds broken and made per 1000 simulation time steps. In both models the ratio of bonds broken to bonds made increases when the strain is applied. (i) The bonds broken in the molecular model increase sharply when strain is applied, which is followed by an increase in bonds made as the ends from previously broken bonds form new ones. (j) The number of bonds broken in the bond topology model also increases at peak stress, followed by an increase in the number of bonds made.

As the resolution of microscopes improves, the alignment of molecules within tissues is likely to become more easily measurable [83,84]. We therefore expect this link between molecule alignment, stress, and bond dynamics to become a powerful tool to probe microscopic properties of tissues.

C. Equilibrium vs enzymatic remodeling

In developing organisms, the collagen IV networks in the BM are subject to stress during growth, but the BM is not isolated. Instead, it is always in contact with cells, which actively secrete proteins and enzymes. Some of these enzymes are known to be involved in collagen IV remodeling and degradation [43,44,85]. Here we explore how the mechanical relaxation and integrity of networks subject to active, enzymaticlike bond remodeling differ from those undergoing equilibrium bond remodeling. In doing so, we restrict ourselves to the bond topology model, because the larger accessible system sizes and timescales make the results more readily comparable to experimental observations of the basement membrane collected in light microscopy imaging and allow us to reduce data noise.

The equilibrium bond remodeling protocol locally satisfies detailed balance, meaning that the ratio between the probabilities of making and breaking a bond obey

$$\frac{P^{\mathrm{EQ}}_{\mathrm{break}}}{P^{\mathrm{EQ}}_{\mathrm{make}}} = \exp(\beta \Delta E), \tag{1}$$

where $\beta = 1/k_B T$, k_B is the Boltzmann constant, T is temperature, and ΔE is the bond energy [Fig. 4(a)]. This relation does not need to hold true for the enzymatic bond remodeling regime where probabilities may depend on other factors such as effective enzyme concentrations and local conformation of the binding sites. For example, mechanosensitive enzymes have been suggested to regulate many other biological

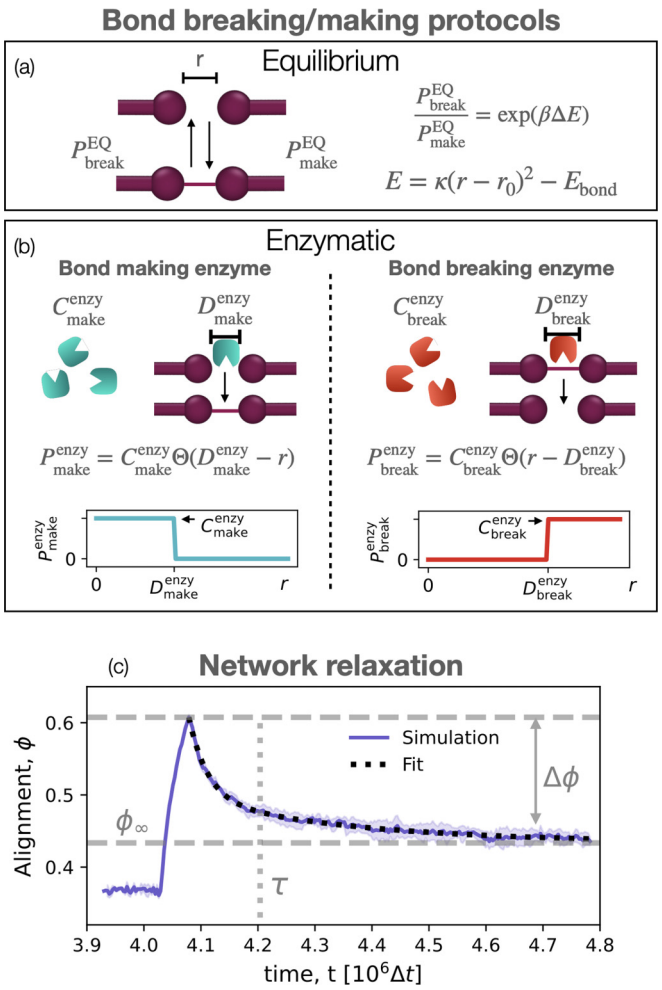

FIG. 4. Bond remodeling protocols and network relaxation. (a) Bond breaking and making protocols in the equilibrium regime. The bonds break and are made with probabilities that satisfy detailed balance [Eq. (1)]. (b) Bond breaking and making protocols in the nonequilibrium/enzymatic regime. The bonds are made or broken with probabilities which are proportional to an effective bond making or breaking enzyme concentration C^{enzy}_{make} or C^{enzy}_{break}, respectively. The fictive enzyme is only active when two ends are within the enzyme activation range, defined by distances D^{enzy}_{make} and D^{enzy}_{break}. (c) Network alignment relaxation in response to strain, with the fit as described in Eq. (4).

filaments and networks such as ESCRT [86] and actin [87]. Additionally, enzymes from the family of matrix metalloproteinases, known to degrade different types of collagen, have been found to act in a strain-dependent manner [88–90]. The nonequilibrium protocol we choose takes inspiration from these mechanosensitive enzymes, which may have different affinities for stretched and relaxed target domains. We model enzymatic remodeling assuming the probabilities for bond making and breaking

$$P^{enzy}_{make} = C^{enzy}_{make}\Theta\left(D^{enzy}_{make} - r\right), \tag{2}$$

$$P^{enzy}_{break} = C^{enzy}_{break}\Theta\left(r - D^{enzy}_{break}\right), \tag{3}$$

where C^{enzy}_{make} and C^{enzy}_{break} are effective parameters representing the concentration of bond making and breaking enzymes, Θ is the Heaviside step function, and r is the bond length, which is a probe for the binding site strain. Enzymes therefore create bonds when two ends from different protomers come closer than the activation distance D^{enzy}_{make} and break bonds when two ends are stretched further apart than the activation distance D^{enzy}_{break} [Fig. 4(b)].

We quantify the relaxation dynamics by measuring the average molecule alignment in the direction of strain, $\phi = \langle\cos^2\theta\rangle$, a robust and relatively noise-free measurement [see Fig. 3(h)]. Similar to the stress relaxation, the alignment response follows a double-exponential decay, shown by the fitting curve in Fig. 4(c),

$$\phi = \phi_\infty + \Delta\phi[f\ \mathrm{e}^{-t/\tau_1} + (1-f)\ \mathrm{e}^{-t/\tau_2}], \tag{4}$$

where relaxation times τ_1 and τ_2, the amplitude ratio f, and the long-time residual alignment ϕ_∞ are fitting parameters. The amount of relaxation $\Delta\phi$ is measured from the alignment curves. We define the overall relaxation time as the amplitude-weighted relaxation time $\tau = f\tau_1 + (1-f)\tau_2$. Representing the relaxation response using these parameters allows us to summarize the effects on relaxation of the bond remodeling parameters and protocol.

When bonds are remodeled following the equilibrium protocol, we find a strong correlation between the amount of network relaxation $\Delta\phi$ and the percentage of protomers *not* in the largest cluster at long times, $\bar{f}_{LC} = 100 - f_{LC}$, which is a probe for network fragmentation. We will refer to this quantity as "fragmentation" for simplicity. In particular, the amount of relaxation scaled by the strain S, $\Delta\tilde{\phi} = \Delta\phi/S$, which we hereafter call simply relaxation amount, collapses to a single line when plotted against fragmentation [Fig. 5(a)]. The networks are less fragmented if the chemical bond energy E_{bond} is larger (shown in different colors in Fig. 5(a)) and this results in a higher initial alignment of the networks and therefore higher $\Delta\tilde{\phi}$. This scaling holds across different applied strains, which are represented by different symbols in Fig. 5(a). Additionally, the amount of network relaxation is also correlated with the speed of relaxation: The networks with higher bond energies E_{bond} have slower bond remodeling dynamics and therefore take longer to relax. This is shown in Fig. 5(b) and is again independent of the amount of strain.

We note that equilibrium networks fall into two distinct regimes. Those with $E_{bond} \lesssim 8k_BT$ undergo continuous thermally driven bond rearrangement, while those with $E_{bond} \gtrsim 8k_BT$ are kinetically trapped and are rearranged only under applied strain. If collagen IV networks remodel via equilibrium mechanisms, they likely fall into the latter regime, as their covalent and disulphide bonds exceed $8k_BT$ [91]. This is in line with other observations of collagen IV networks *in vitro*, which have 3.2 bonds per protomer [58], a value we observe in the high-bond-energy limit. In contrast, low-bond-energy networks show a higher number of bonds per protomer (Fig. S9D in the SM [73]).

The enzymatic regime deviates from the equilibrium regime in two significant ways. First, while in equilibrium the bond dynamics is constrained by the bond energy through detailed balance as per Eq. (1), out-of-equilibrium bond making and bond breaking are fully independent and regulated by distinct quantities. We observe that the relaxation

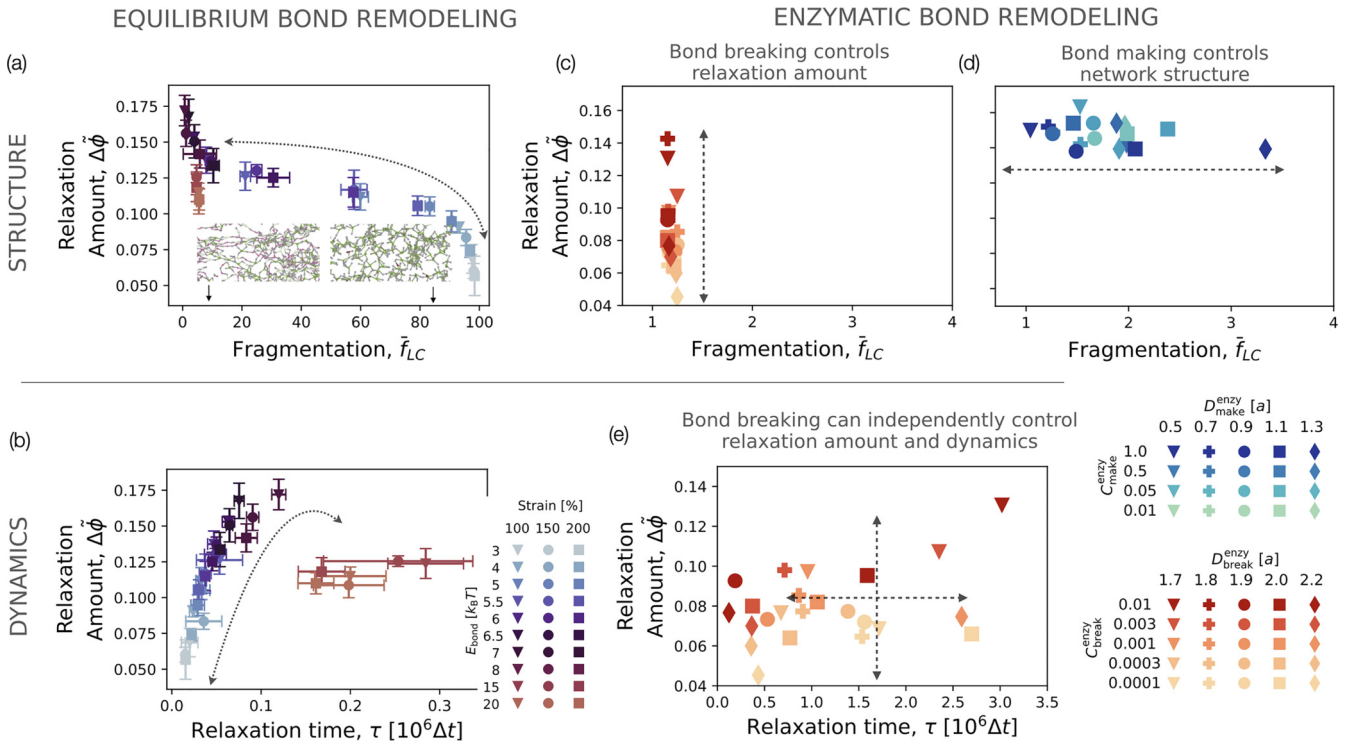

FIG. 5. Relaxation dynamics for equilibrium and enzymatic bond remodeling. (a) and (b) Equilibrium regime. Amount of network relaxation scaled by the strain, $\Delta\tilde{\phi}$, as a function of (a) the percentage of the network not in the largest connected cluster $\bar{f}_{LC}$ and (b) the relaxation timescale τ, for different amounts of strain and chemical bond energies E_{bond}. Bottom snapshots in (a) show networks with low (left) and high (right) fragmentation. Both panels share the legend shown in (b). The error bars are the standard deviation calculated from five random seeds. (c)–(e) Enzymatic regime. $\Delta\tilde{\phi}$ as a function of the network fragmentation $\bar{f}_{LC}$ for varying bond breaking (c) and making (d) parameters. Different concentration of enzymes, $C^{\text{enzy}}_{\text{break}}$ and $C^{\text{enzy}}_{\text{make}}$, are represented by different colors and different activation distances, $D^{\text{enzy}}_{\text{break}}$ and $D^{\text{enzy}}_{\text{make}}$, by different symbols. (e) $\Delta\tilde{\phi}$ as a function of τ for the same bond breaking parameters as in (c). For (c) and (e) the strain is 150%, $D^{\text{enzy}}_{\text{make}} = 0.65a$, and $C^{\text{enzy}}_{\text{make}} = 1.0$. For (d) the strain is 150%, $D^{\text{enzy}}_{\text{break}} = 1.8a$, and $C^{\text{enzy}}_{\text{break}} = 0.1$.

dynamics is essentially determined by bond breaking enzymes, whereas bond making enzymes govern network connectivity. This means that within enzymatic remodeling, the correlation between connectivity and the amount the network relaxes, seen in Fig. 5(a) for the equilibrium regime, does not have to hold.

This is evident in Fig. 5(d), where by varying the bond making activation distance $D^{\text{enzy}}_{\text{make}}$ (symbols) or the concentration of bond making enzymes $C^{\text{enzy}}_{\text{make}}$ (colors), the system deviates from the connectivity prescribed by equilibrium. Additionally, varying the bond breaking parameters determines the amount of relaxation $\Delta\tilde{\phi}$ independently of connectivity [Fig. 5(c)]. This means that enzymatic bond remodeling allows stress to relax without compromising the structural integrity of the network. Varying the concentration of breaking and making enzymes, one can cover more of the phase space represented in Figs. 5(c) and 5(d) without fragmenting the network, whereas at equilibrium the available phase space is constrained [Fig. 5(a)].

The second way in which the enzymatic regime deviates from the equilibrium regime is more subtle. In the equilibrium regime, one parameter controls the frequency of bond breaking: the bond energy. In the enzymatic regime, there are two parameters contributing to this frequency: the bond breaking probability $C^{\text{enzy}}_{\text{break}}$ and the bond breaking activation distance $D^{\text{enzy}}_{\text{break}}$. The overall frequency of bond breaking is proportional to $C^{\text{enzy}}_{\text{break}} \exp[-E(D^{\text{enzy}}_{\text{break}})]$, where the first term is the probability of a bond within activation distance to break and the second term is the probability of being within activation distance (modulo a constant). Therefore, the same overall bond breaking frequency can be obtained by different combinations of the bond breaking parameters $C^{\text{enzy}}_{\text{break}}$ and $D^{\text{enzy}}_{\text{break}}$, meaning that the system can be more or less sensitive to how stretched bonds are.

When an enzyme only breaks stretched bonds (large $D^{\text{enzy}}_{\text{break}}$), networks relax faster: The breaking of stretched bonds, as opposed to that of unstretched bonds, drives stress relaxation. This is clear from Fig. 5(e), where the different colors represent the enzyme concentration and the different symbols represent the bond breaking activation distance. In this graph, the colors broadly dictate the amount of relaxation, while the symbols contribute to determine the timescale of relaxation.

Once more, varying the breaking parameters allows the tiling of the whole phase space in Fig. 5(e), unlocking relaxation pathways that are unachievable in equilibrium [Fig. 5(b)]. In summary, in the enzymatic regime the relaxation timescales can be tuned independently of the amount of relaxation, while in the equilibrium case these are intrinsically coupled.

It is possible to implement the bond remodeling in the enzymatic regime such that it is nonmechanosensitive. This is the extreme case where the bond breaking activation distance $D_{\text{break}}^{\text{enzy}}$ becomes zero and any bond may be broken. The enzyme concentration in this case is the only parameter dictating the bond breaking dynamics. The results for nonmechanosensitive bond remodeling are shown in Fig. S10 in the SM [73], showing that these networks can also relax with a range of timescales and amounts while keeping fully connected.

IV. DISCUSSION

We presented the first computational framework to investigate how the mechanics and dynamics of the basement membrane may be influenced by collagen IV bond remodeling and the activity of enzymes. By developing two models of collagen IV with two different levels of coarse graining, we investigated the connectivity of percolating collagen IV networks and linked this to experimental observations. We then applied a step strain to the networks to measure the stress response. We found that in the regime of high strain the relaxation dynamics in both models are dominated by bond remodeling, meaning that the networks relieve stress by breaking and reforming bonds. Within this regime, we systematically explored different protocols for bond remodeling using the more-coarse-grained model. We compared equilibrium and enzymatic bond remodeling protocols, where enzymatic protocols are not constrained to satisfy equilibrium thermodynamics. A key finding is that in equilibrium, there is an interdependence between the amount of stress relaxation the network can undergo, its structural integrity, and the typical relaxation time. In other words, these different physical quantities cannot be tuned independently. Enzymatic bond remodeling, however, is not restricted in such a way, so relaxation pathways are available that are inaccessible in equilibrium.

This is a powerful result showing that materials forming and developing while consuming energy have different and more diverse mechanical properties than their passive counterparts. Previous studies on various systems have demonstrated that structures assembled out of equilibrium show a signature of broken detailed balance through nonzero currents in phase space, large-scale fluctuations, or unusual mechanical responses, even once activity has stopped [68,70,71,92]. In general, there are many possible ways of identifying nonequilibrium signatures. Here we showed that an underexplored approach is to analyze the relations between network fragmentation and relaxation dynamics. This new metric for nonequilibrium is particularly promising, as it can in principle be checked for in experiment; it relies only on measuring how alignment varies in time under strain and might allow us to infer microscopic remodeling mechanisms from macroscopic observations.

The concentrations and mechanosensitive properties of bond-cleaving enzymes emerge as free parameters and are capable, in principle, of tuning the structure and mechanics of the network. This may be crucial in biology, especially in developing organisms where large shape changes must occur in a controlled manner [93]. For example, the collagen IV network in the basement membrane of a developing tissue provides mechanical stiffness on short timescales, but must relax on the timescale of tissue growth [41]. Using enzymes, an organism could achieve precise timescales of relaxation and amount of relaxation, while keeping network integrity. Additionally, during development, the basement membrane properties may change in time by simply changing enzyme activity, rather than needing to change the chemical nature of the network itself. Without enzymatic activity, the material is restricted to mechanical properties which are solely governed by the chemistry and connectivity of the underlying network. We envisage that a future direction of this work will be to further understand the changes in basement membrane mechanics due to aging [36,94,95], disease [96], or drugs [97], which all could be due to changes in enzyme activity and collagen IV turnover.

It should be noted that there are numerous ways in which active systems may deviate from equilibrium bond remodeling kinetics, and we chose here just one, where enzymes actively break and make bonds depending on bond distance or else randomly. Other examples might include the action of bond swapping, whereby the number of bonds in the network stays strictly constant but energy is consumed to swap bonds between neighbors, similar to vitrimer networks [27]. Another mechanism is present in actively cross-linked bionetworks like actomyosin, where structural changes may be caused by bond sliding using the action of walking motors [31].

We here chose a simple realization of bond remodeling, where both NC1 bonds and 7S bonds can be broken and made, and the triple helix chain is never broken. This assumption is likely valid for equilibrium bond remodeling because the intraprotomer bonds of the triple helix are more stable than the interprotomer bonds [98]. However, enzymes like collagenase could degrade collagen IV networks in other ways and may well degrade the triple helix [99], which would be less likely to rebind into a network. We note that if enzymes degrade the protomers' binding domain, such that the second neighbors in the network are free to rebind [42], the model proposed here remains a good approximation. We break bonds one at a time, though the results would not be significantly different if we were to break the two protomer bonds simultaneously.

The methods and models introduced here should be considered as a minimal framework to explore and contrast the active and passive remodeling of collagen IV networks. Systematically exploring other nonequilibrium bond remodeling regimes and their effects on the mechanics of networks is a compelling future direction. This development would be in tandem with ever-improving experimental techniques in mechanobiology which hold great promise to elucidate the nonequilibrium mechanism behind bond remodeling of collagen IV *in vivo*.

ACKNOWLEDGMENTS

This work received funding from the European Research Council under the European Union's Horizon 2020 research and innovation program through Grant Agreement No. 802960 (B.M., V.S., I.P., and A.Š.), the European Union's Horizon 2020 research and innovation program under the Marie Skłodowska-Curie Grant Agreement No. 101034413 (I.P.), the NOMIS Foundation (F.P.-V.), the National Centre

for the Replacement, Refinement and Reduction of Animals in Research Grant No. NC/T002425/1 (N.K.), Leverhulme Trust project Grant No. RPG-2020-068 (N.K.), MRC Fellowship No. MR/W027437/1 (Y.M.), a Lister Institute Research Prize (Y.M.) and EMBO Young Investigator Programme (Y.M. and A.Š.).

[1] R. Jayadev and D. R. Sherwood, Basement membranes, Curr. Biol. **27**, R207 (2017).

[2] A. L. Fidler, C. E. Darris, S. V. Chetyrkin, V. K. Pedchenko, S. P. Boudko, K. L. Brown, W. Gray Jerome, J. K. Hudson, A. Rokas, and B. G. Hudson, Collagen IV and basement membrane at the evolutionary dawn of metazoan tissues, eLife **6**, e24176 (2017).

[3] N. Khalilgharibi and Y. Mao, To form and function: on the role of basement membrane mechanics in tissue development, homeostasis and disease, Open Biol. **11**, 200360 (2021).

[4] M. A. Morrissey and D. R. Sherwood, An active role for basement membrane assembly and modification in tissue sculpting, J. Cell Sci. **128**, 1661 (2015).

[5] D.-Y. Chen, J. Crest, S. J. Streichan, and D. Bilder, Extracellular matrix stiffness cues junctional remodeling for 3D tissue elongation, Nat. Commun. **10**, 3339 (2019).

[6] J. Candiello, G. J. Cole, and W. Halfter, Age-dependent changes in the structure, composition and biophysical properties of a human basement membrane, Matrix Biol. **29**, 402 (2010).

[7] O. Uspenskaia, M. Liebetrau, J. Herms, A. Danek, and G. F. Hamann, Aging is associated with increased collagen type IV accumulation in the basal lamina of human cerebral microvessels, BMC Neurosci. **5**, 37 (2004).

[8] O. Chaudhuri, J. Cooper-White, P. A. Janmey, D. J. Mooney, and V. B. Shenoy, Effects of extracellular matrix viscoelasticity on cellular behaviour, Nature (London) **584**, 535 (2020).

[9] J. J. Grantham, V. S. Donoso, A. P. Evan, F. A. Carone, and K. D. Gardner, Viscoelastic properties of tubule basement membranes in experimental renal cystic disease, Kidney Int. **32**, 187 (1987).

[10] A. Elosegui-Artola, A. Gupta, A. J. Najibi, B. R. Seo, R. Garry, C. M. Tringides, I. De Lázaro, M. Darnell, W. Gu, Q. Zhou, D. A. Weitz, L. Mahadevan, and D. J. Mooney, Matrix viscoelasticity controls spatiotemporal tissue organization, Nat. Mater. **22**, 117 (2023).

[11] S. Nam, J. Lee, D. Brownfield, and O. Chaudhuri, Viscoplasticity enables mechanical remodeling of matrix by cells, Biophys. J. **111**, 2296 (2016).

[12] L. E. Malvern, *Introduction to the Mechanics of a Continuous Medium* (Prentice-Hall, Englewood Cliffs, 1969).

[13] M. Doi and S. F. Edwards, *The Theory of Polymer Dynamics* (Oxford University Press, Oxford, 1986).

[14] P.-G. de Gennes, *Scaling Concepts in Polymer Physics* (Cornell University Press, Ithaca, 1979).

[15] M. Rubinstein and R. H. Colby, *Polymer Physics* (Oxford University Press, Oxford, 2003).

[16] A. E. Likhtman, S. K. Sukumaran, and J. Ramirez, Linear viscoelasticity from molecular dynamics simulation of entangled polymers, Macromolecules **40**, 6748 (2007).

[17] J.-X. Hou, C. Svaneborg, R. Everaers, and G. S. Grest, Stress relaxation in entangled polymer melts, Phys. Rev. Lett. **105**, 068301 (2010).

[18] L. Leibler, M. Rubinstein, and R. H. Colby, Dynamics of reversible networks, Macromolecules **24**, 4701 (1991).

[19] E. B. Stukalin, L.-H. Cai, N. A. Kumar, L. Leibler, and M. Rubinstein, Self-healing of unentangled polymer networks with reversible bonds, Macromolecules **46**, 7525 (2013).

[20] S. Wang and M. W. Urban, Self-healing polymers, Nat. Rev. Mater. **5**, 562 (2020).

[21] R. J. Wagner, E. Hobbs, and F. J. Vernerey, A network model of transient polymers: exploring the micromechanics of nonlinear viscoelasticity, Soft Matter **17**, 8742 (2021).

[22] R. J. Wagner and M. N. Silberstein, A foundational framework for the mesoscale modeling of dynamic elastomers and gels, J. Mech. Phys. Solids **194**, 105914 (2025).

[23] P. Cordier, F. Tournilhac, C. Soulié-Ziakovic, and L. Leibler, Self-healing and thermoreversible rubber from supramolecular assembly, Nature (London) **451**, 977 (2008).

[24] C.-H. Li and J.-L. Zuo, Self-healing polymers based on coordination bonds, Adv. Mater. **32**, 1903762 (2020).

[25] D. Montarnal, M. Capelot, F. Tournilhac, and L. Leibler, Silica-like malleable materials from permanent organic networks, Science **334**, 965 (2011).

[26] W. Denissen, J. M. Winne, and F. E. Du Prez, Vitrimers: permanent organic networks with glass-like fluidity, Chem. Sci. **7**, 30 (2016).

[27] F. Meng, M. O. Saed, and E. M. Terentjev, Rheology of vitrimers, Nat. Commun. **13**, 5753 (2022).

[28] H. Zhao, X. Wei, Y. Fang, K. Gao, T. Yue, L. Zhang, V. Ganesan, F. Meng, and J. Liu, Molecular dynamics simulation of the structural, mechanical, and reprocessing properties of Vitrimers based on a dynamic covalent polymer network, Macromolecules **55**, 1091 (2022).

[29] Y.-C. Lin, G. H. Koenderink, F. C. MacKintosh, and D. A. Weitz, Viscoelastic properties of microtubule networks, Macromolecules **40**, 7714 (2007).

[30] S. Forth and T. M. Kapoor, The mechanics of microtubule networks in cell division, J. Cell Biol. **216**, 1525 (2017).

[31] S. Banerjee, M. L. Gardel, and U. S. Schwarz, The actin cytoskeleton as an active adaptive material, Annu. Rev. Condens. Matter Phys. **11**, 421 (2020).

[32] F. Burla, Y. Mulla, B. E. Vos, A. Aufderhorst-Roberts, and G. H. Koenderink, From mechanical resilience to active material properties in biopolymer networks, Nat. Rev. Phys. **1**, 249 (2019).

[33] R. J. Wagner, S. C. Lamont, Z. T. White, and F. J. Vernerey, Catch bond kinetics are instrumental to cohesion of fire ant rafts under load, Proc. Natl. Acad. Sci. USA **121**, e2314772121 (2024).

[34] R. Price and R. Spiro, Studies on the metabolism of the renal glomerular basement membrane, J. Biol. Chem. **252**, 8597 (1977).

[35] Y. Matsubayashi, B. J. Sánchez-Sánchez, S. Marcotti, E. Serna-Morales, A. Dragu, M.-d.-C. Díaz-de-la Loza, G. Vizcay-Barrena, R. A. Fleck, and B. M. Stramer, Rapid homeostatic

turnover of embryonic ECM during tissue morphogenesis, Dev. Cell **54**, 33 (2020).

[36] S. N. Kehlet, N. Willumsen, G. Armbrecht, R. Dietzel, S. Brix, K. Henriksen, and M. A. Karsdal, Age-related collagen turnover of the interstitial matrix and basement membrane: Implications of age- and sex-dependent remodeling of the extracellular matrix, PLoS One **13**, e0194458 (2018).

[37] R. Kalluri, C. F. Shield, P. Todd, B. G. Hudson, and E. G. Neilson, Isoform switching of type IV collagen is developmentally arrested in X-linked Alport syndrome leading to increased susceptibility of renal basement membranes to endoproteolysis, J. Clin. Invest. **99**, 2470 (1997).

[38] J. M. Sand, L. Larsen, C. Hogaboam, F. Martinez, M. Han, M. R. Larsen, A. Nawrocki, Q. Zheng, M. A. Karsdal, and D. J. Leeming, MMP mediated degradation of type IV collagen alpha 1 and alpha 3 chains reflects basement membrane remodeling in experimental and clinical fibrosis – validation of two novel biomarker assays, PLoS One **8**, e84934 (2013).

[39] D. G. K. Rasmussen, L. Boesby, S. H. Nielsen, M. Tepel, S. Birot, M. A. Karsdal, A.-L. Kamper, and F. Genovese, Collagen turnover profiles in chronic kidney disease, Sci. Rep. **9**, 16062 (2019).

[40] A. R. Bourgonje, M. S. Alexdottir, A. T. Otten, R. Loveikyte, A.-C. Bay-Jensen, M. Pehrsson, H. M. van Dullemen, M. C. Visschedijk, E. A. M. Festen, R. K. Weersma, M. A. Karsdal, K. N. Faber, J. H. Mortensen, and G. Dijkstra, Serological biomarkers of type I, III and IV collagen turnover are associated with the presence and future progression of stricturing and penetrating Crohn's disease, Aliment. Pharmacol. Ther. **56**, 675 (2022).

[41] K. Y. Guerra Santillán, C. Dahmann, and E. Fischer-Friedrich, Elastic contractile stress in the basement membrane generates basal tension in Epithelia, PRX Life **2**, 013004 (2024).

[42] I. T. Rebustini, C. Myers, K. S. Lassiter, A. Surmak, L. Szabova, K. Holmbeck, V. Pedchenko, B. G. Hudson, and M. P. Hoffman, MT2-MMP-dependent release of collagen IV NC1 domains regulates submandibular gland branching morphogenesis, Dev. Cell **17**, 482 (2009).

[43] M. Arden, M. Spearman, and I. Adamson, Degradation of type IV collagen during the development of fetal rat lung, Am. J. Respir. Cell Mol. Biol. **9**, 99 (1993).

[44] A. C. Curino, L. H. Engelholm, S. S. Yamada, K. Holmbeck, L. R. Lund, A. A. Molinolo, N. Behrendt, B. S. Nielsen, and T. H. Bugge, Intracellular collagen degradation mediated by uPARAP/Endo180 is a major pathway of extracellular matrix turnover during malignancy, J. Cell Biol. **169**, 977 (2005).

[45] R. A. Wyatt and B. D. Crawford, Post-translational activation of Mmp2 correlates with patterns of active collagen degradation during the development of the zebrafish tail, Dev. Biol. **477**, 155 (2021).

[46] V. J. Huber, H. Igarashi, S. Ueki, M. Terumitsu-Tsujita, C. Nito, K. Ohno, Y. Suzuki, K. Itoh, I. L. Kwee, and T. Nakada, Visualizing the distribution of matrix metalloproteinases in Ischemic brain using In Vivo 19F-magnetic resonance spectroscopic imaging, Contrast Media Mol. Imag. **2019**, 1 (2019).

[47] A. O'Hara, F.-L. Lim, D. J. Mazzatti, and P. Trayhurn, Microarray analysis identifies matrix metalloproteinases (MMPs) as key genes whose expression is up-regulated in human adipocytes by macrophage-conditioned medium, Pflug. Arch. Eur. J. Physiol. **458**, 1103 (2009).

[48] B. N. Narasimhan and S. I. Fraley, Degradability tunes ECM stress relaxation and cellular mechanics, bioRxiv (2024), doi:10.1101/2024.07.28.605514.

[49] S. K. Ranamukhaarachchi, A. Walker, M.-H. Tang, W. D. Leineweber, S. Lam, W.-J. Rappel, and S. I. Fraley, Global versus local matrix remodeling drives rotational versus invasive collective migration of epithelial cells, Dev. Cell **60**, 871 (2024).

[50] J. Khoshnoodi, V. Pedchenko, and B. G. Hudson, Mammalian collagen IV, Microsc. Res. Tech. **71**, 357 (2008).

[51] A. Al-Shaer and N. R. Forde, Decoding collagens thermally induced unfolding and refolding pathways, Proc. Natl. Acad. Sci. USA **122**, e2420308122 (2025).

[52] A. M. Abreu-Velez and M. S. Howard, Collagen IV in normal skin and in pathological processes, N. Am. J. Med. Sci. **4**, 1 (2012).

[53] M. E. Than, S. Henrich, R. Huber, A. Ries, K. Mann, K. Kühn, R. Timpl, G. P. Bourenkov, H. D. Bartunik, and W. Bode, The 1.9-Å crystal structure of the noncollagenous (NC1) domain of human placenta collagen IV shows stabilization via a novel type of covalent Met-Lys cross-link, Proc. Natl. Acad. Sci. USA **99**, 6607 (2002).

[54] M. Sundaramoorthy, M. Meiyappan, P. Todd, and B. G. Hudson, Crystal structure of NC1 domains structural basis for type IV collagen assembly in basement membranes, J. Biol. Chem. **277**, 31142 (2002).

[55] K. Kühn, H. Wiedemann, R. Timpl, J. Risteli, H. Dieringer, T. Voss, and R. W. Glanville, Macromolecular structure of basement membrane collagens, FEBS Lett. **125**, 123 (1981).

[56] R. Timpl, H. Wiedemann, V. Delden, H. Furthmayr, and K. Kuhn, A network model for the organization of type IV collagen molecules in basement membranes, Eur. J. Biochem. **120**, 203 (1981).

[57] R. Kalluri and D. Cosgrove, Assembly of type IV collagen insights from α_3(IV) collagen-deficient mice, J. Biol. Chem. **275**, 12719 (2000).

[58] P. D. Yurchenco and H. Furthmayr, Type IV collagen "7S" tetramer formation: Aspects of kinetics and thermodynamics, Ann. N.Y. Acad. Sci. **460**, 530 (1985).

[59] A. J. Licup, S. Münster, A. Sharma, M. Sheinman, L. M. Jawerth, B. Fabry, D. A. Weitz, and F. C. MacKintosh, Stress controls the mechanics of collagen networks, Proc. Natl. Acad. Sci. USA **112**, 9573 (2015).

[60] K. A. Jansen, A. J. Licup, A. Sharma, R. Rens, F. C. MacKintosh, and G. H. Koenderink, The role of network architecture in collagen mechanics, Biophys. J. **114**, 2665 (2018).

[61] C. P. Broedersz and F. C. MacKintosh, Modeling semiflexible polymer networks, Rev. Mod. Phys. **86**, 995 (2014).

[62] A. E. Hafner, N. G. Gyori, C. A. Bench, L. K. Davis, and A. Šarić, Modeling fibrillogenesis of collagen-mimetic molecules, Biophys. J. **119**, 1791 (2020).

[63] H. J. Burd, A structural constitutive model for the human lens capsule, Biomech. Model. Mechanobiol. **8**, 217 (2009).

[64] M. H. J. Bailey and M. Wilson, Simulation of defects, flexibility and rupture in biopolymer networks, RSC Adv. **12**, 2171 (2022).

[65] A. E. Hafner, J. Krausser, and A. Šarić, Minimal coarse-grained models for molecular self-organisation in biology, Curr. Opin. Struct. Biol. **58**, 43 (2019).

[66] M. E. Tuckerman, *Statistical Mechanics: Theory and Molecular Simulation* (Oxford University Press, Oxford, 2023).

[67] F. S. Gnesotto, F. Mura, J. Gladrow, and C. P. Broedersz, Broken detailed balance and non-equilibrium dynamics in living systems: A review, Rep. Prog. Phys. **81**, 066601 (2018).

[68] D. Mizuno, C. Tardin, C. F. Schmidt, and F. C. MacKintosh, Nonequilibrium mechanics of active cytoskeletal networks, Science **315**, 370 (2007).

[69] A. J. Levine and F. C. MacKintosh, The mechanics and fluctuation spectrum of active gels, J. Phys. Chem. B **113**, 3820 (2009).

[70] Y. Shi, C. L. Porter, J. C. Crocker, and D. H. Reich, Dissecting fat-tailed fluctuations in the cytoskeleton with active micropost arrays, Proc. Natl. Acad. Sci. USA **116**, 13839 (2019).

[71] D. Grober, I. Palaia, M. C. Uçar, E. Hannezo, A. Šarić, and J. Palacci, Unconventional colloidal aggregation in chiral bacterial baths, Nat. Phys. **19**, 1680 (2023).

[72] B. Siebold, R.-q. Qian, R. W. Glanville, H. Hofmann, R. Deutzmann, and K. Kähn, Construction of a model for the aggregation and cross-linking region (7S domain) of type IV collagen based upon an evaluation of the primary structure of the $\alpha 1$ and $\alpha 2$ chains in this region, Eur. J. Biochem. **168**, 569 (1987).

[73] See Supplemental Material at http://link.aps.org/supplemental/10.1103/gdd5-rnh7 for further model details, additional figures and captions for videos 1–4.

[74] D. Frenkel and B. Smit, *Understanding Molecular Simulation: From Algorithms to Applications* (Elsevier, Amsterdam, 2023).

[75] T. Schneider and E. Stoll, Molecular-dynamics study of a three-dimensional one-component model for distortive phase transitions, Phys. Rev. B **17**, 1302 (1978).

[76] A. P. Thompson, H. M. Aktulga, R. Berger, D. S. Bolintineanu, W. M. Brown, P. S. Crozier, P. J. in 't Veld, A. Kohlmeyer, S. G. Moore, T. D. Nguyen, R. Shan, M. J. Stevens, J. Tranchida, C. Trott, and S. J. Plimpton, LAMMPS - a flexible simulation tool for particle-based materials modeling at the atomic, meso, and continuum scales, Comput. Phys. Commun. **271**, 108171 (2022).

[77] A. Stukowski, Visualization and analysis of atomistic simulation data with OVITO—the open visualization tool, Model. Simul. Mater. Sci. Eng. **18**, 015012 (2010).

[78] J. R. Gissinger, B. D. Jensen, and K. E. Wise, REACTER: A Heuristic method for reactive molecular dynamics, Macromolecules **53**, 9953 (2020).

[79] K. Barnard, S. A. Burgess, D. A. Carter, and D. M. Woolley, Three-dimensional structure of type IV collagen in the mammalian lens capsule, J. Struct. Biol. **108**, 6 (1992).

[80] M. Duda, N. J. Kirkland, N. Khalilgharibi, M. Tozluoglu, A. C. Yuen, N. Carpi, A. Bove, M. Piel, G. Charras, B. Baum, and Y. Mao, Polarization of Myosin II refines tissue material properties to buffer mechanical stress, Dev. Cell **48**, 245 (2019).

[81] C.-T. Lee and M. Merkel, Stiffening of under-constrained spring networks under isotropic strain, Soft Matter **18**, 5410 (2022).

[82] S. Dar, R. Tesoro Moreno, I. van Palaia, A. B. Gopalan, Z. G. Sun, L. Strauss, R. Springer, J. M. Belmonte, S. K. Foster, M. Murrell, C. S. Ejsing, A. Šarić, M. Leptin, and A. Diz-Muñoz, Caging of membrane-to-cortex attachment proteins can trigger cellular symmetry breaking, bioRxiv (2024), doi:10.1101/2024.10.14.618153.

[83] C. A. V. Cruz, H. A. Shaban, A. Kress, N. Bertaux, S. Monneret, M. Mavrakis, J. Savatier, and S. Brasselet, Quantitative nanoscale imaging of orientational order in biological filaments by polarized superresolution microscopy, Proc. Natl. Acad. Sci. USA **113**, E820 (2016).

[84] A. S. Piotrowski-Daspit, B. A. Nerger, A. E. Wolf, S. Sundaresan, and C. M. Nelson, Dynamics of tissue-induced alignment of fibrous extracellular matrix, Biophys. J. **113**, 702 (2017).

[85] C. Monteagudo, M. J. Merino, J. San-Juan, L. A. Liotta, and W. G. Stetler-Stevenson, Immunohistochemical distribution of type IV collagenase in normal, benign, and malignant breast tissue, Am. J. Pathol. **136**, 585 (1990).

[86] B. Meadowcroft, I. Palaia, A.-K. Pfitzner, A. Roux, B. Baum, and A. Šarić, Mechanochemical rules for shape-shifting filaments that remodel membranes, Phys. Rev. Lett. **129**, 268101 (2022).

[87] K. Hayakawa, H. Tatsumi, and M. Sokabe, Actin filaments function as a tension sensor by tension-dependent binding of cofilin to the filament, J. Cell Biol. **195**, 721 (2011).

[88] S.-W. Chang, B. P. Flynn, J. W. Ruberti, and M. J. Buehler, Molecular mechanism of force induced stabilization of collagen against enzymatic breakdown, Biomaterials **33**, 3852 (2012).

[89] A. S. Adhikari, J. Chai, and A. R. Dunn, Mechanical load induces a 100-fold increase in the rate of collagen proteolysis by MMP-1, J. Am. Chem. Soc. **133**, 1686 (2011).

[90] B. P. Flynn, A. P. Bhole, N. Saeidi, M. Liles, C. A. DiMarzio, and J. W. Ruberti, Mechanical strain stabilizes reconstituted collagen fibrils against enzymatic degradation by mammalian collagenase matrix metalloproteinase 8 (MMP-8), PLoS One **5**, e12337 (2010).

[91] K. L. Brown, C. F. Cummings, R. M. Vanacore, and B. G. Hudson, Building collagen IV smart scaffolds on the outside of cells, Protein Sci. **26**, 2151 (2017).

[92] C. Battle, C. P. Broedersz, N. Fakhri, V. F. Geyer, J. Howard, C. F. Schmidt, and F. C. MacKintosh, Broken detailed balance at mesoscopic scales in active biological systems, Science **352**, 604 (2016).

[93] G. Paci and Y. Mao, Forced into shape: Mechanical forces in Drosophila development and homeostasis, Semin. Cell Dev. Biol. **120**, 160 (2021).

[94] G. J. Fisher, S. C. Datta, H. S. Talwar, Z.-Q. Wang, J. Varani, S. Kang, and J. J. Voorhees, Molecular basis of sun-induced premature skin ageing and retinoid antagonism, Nature (London) **379**, 335 (1996).

[95] M. A. Karsdal, F. Genovese, E. A. Madsen, T. Manon-Jensen, and D. Schuppan, Collagen and tissue turnover as a function of age: Implications for fibrosis, J. Hepatol. **64**, 103 (2016).

[96] M. Wolosowicz, S. Prokopiuk, and T. W. Kaminski, The complex role of matrix metalloproteinase-2 (MMP-2) in health and disease, Int. J. Mol. Sci. **25**, 13691 (2024).

[97] X. Lu, L. Ding, H. Song, W. Yu, C. Dong, and J. Ren, *In situ* quantitative measurements on MMP-9 activity in single living cells by single molecule fluorescence correlation spectroscopy, Analyst **148**, 752 (2023).

[98] A. L. Fidler, S. P. Boudko, A. Rokas, and B. G. Hudson, The triple helix of collagens – an ancient protein structure that enabled animal multicellularity and tissue evolution, J. Cell Sci. **131**, jcs203950 (2018).

[99] L. M. Matrisian, The matrix-degrading metalloproteinases, BioEssays **14**, 455 (1992).